REVIEW

National Science Open
1: 20220025, 2022
https://doi.org/10.1360/nso/20220025

Earth and Environmental Sciences
Special Topic: Emerging Pollution and Emerging Pollutants

Advances and challenges of photocatalytic technology for air purification

Qin Geng[1], Hong Wang[2], Ruiming Chen[2], Lvcun Chen[1], Kanglu Li[1] & Fan Dong[1,2,*]

[1]*Yangtze Delta Region Institute (Huzhou), University of Electronic Science and Technology of China, Huzhou 313000, China;*
[2]*Research Center for Environmental and Energy Catalysis, Institute of Fundamental and Frontier Sciences, University of Electronic Science and Technology of China, Chengdu 611731, China*

Received 6 February 2022; Revised 20 June 2022; Accepted 23 June 2022; Published online 2 September 2022

Abstract: With the acceleration of the urban industrialization process, air pollutant emission has increased sharply, which seriously endangers the ecological environment and human beings. Solar-driven photocatalysis has the broad-spectrum activity for various inorganic to organic pollutants at ambient temperature without harsh reaction conditions, which shows a very broad application prospect in air purification. However, the photocatalysis technology suffers from the unrevealed reaction mechanism and the deactivation of photocatalysts, which severely limits its practical application. Currently, there is still a huge gap between basic research and industrial application in the field of photocatalytic air purification. This review summarizes recent progress on photocatalytic degradation of air pollutants and categorizes them based on the types of photocatalytic materials and air pollutants, with a focus on photocatalytic reaction mechanisms and the application scenarios of photocatalytic air purification to identify this gap. We also critically discussed the major challenges for promoting applications of photocatalytic technology and put forward the development prospect.

Keywords: photocatalytic technology, air purification, air pollutants, reaction pathways, application scenarios

Introduction

It is well known that urbanization and industrialization have resulted in rapidly increasing emissions of air pollutions (e.g., volatile organic compounds (VOCs), nitrogen-containing compounds (NO_x), and sulfur dioxide (SO_2)) [1–5]. Most emitted air pollution can lead to the formation of secondary pollutants (e.g., tropospheric ozone, peroxyacetyl nitrate), secondary organic aerosols, and photochemical smog [6,7], which is the major cause of a sharp decrease in air quality in numerous regions around the world [8–10]. Long-term exposure to air pollutants induces respiratory diseases and increases the incidence of respiratory diseases and cancer [11–14]. Besides, air pollutants also pose a serious threat to the survival and well-being of local plants and animals. According to the World Health Organization health report, in 2012, air pollution caused about 7 million deaths worldwide, of which 3.7 million were caused by outdoor pollution, 4.3 million by indoor pollution, and the remaining 1 million by a combination of the above both. There are manifold research initiatives currently under development to meet the challenging air pollution problem. Adsorption tech-

nology is the leading approach for air purification currently [15]. However, adsorption capacity remarkably decreases when air pollutions are present at low concentrations (usually sub-ppm levels) [16]. In addition, the replacement, cleaning, and disposal of adsorbent materials are costly processes and may cause secondary pollution. Thermal incineration is also an efficient technology, but it typically requires high temperatures (≥800°C) and consumes high energy [17]. Furthermore, incomplete thermal oxidation of pollutants also produces numerous noxious byproducts. Besides, non-thermal plasma inevitably produces undesirable reaction by-products such as ozone and NO_x [18–20].

Solar-driven photocatalysis is a promising alternative for air purification, which has broad-spectrum activity toward various inorganic to organic pollutants under mild conditions. The principle of photocatalysis is founded on the solid energy band theory [21]. When a semiconductor photocatalyst initiates by an appropriate light source with energy greater than its bandgap energy, the electrons (e^-) can transfer from the valence band (VB) to its conduction band (CB), and then leave holes (h^+) in the corresponding position of the VB. The photogenerated e^- and h^+ will undergo redox reactions with the water/oxygen molecules adsorbed on the surface of the photocatalyst to generate reactive oxygen species (ROS) [22,23]. Subsequently, the adsorbed air pollutants can react with the generated ROS and eventually be oxidized to form a stable end product [24]. In recent years, numerous research results have been reported on the photocatalytic air pollutant degradation technology, and the current research is focused on the design of photocatalytic materials and the mechanism of pollutant degradation [25–28]. The conversation and degradation mechanism of air pollutants requires sufficient research, which is essential for elevating the overall photocatalytic efficiency. Hu *et al*. [29] synthesized a single-atom Au-supported TiO_2 photocatalyst to expand the light absorption performance and enhance the photocatalytic degradation efficiency of acetone. He *et al*. [30] reported a strategy to introduce an *in-situ* water layer on WO_3 by coating hygroscopic periodic acid to dramatically enhance the photocatalytic removal of hydrophilic VOCs (formaldehyde (CH_2O) and acetone) in the air. Dong and co-workers [31] comprehensively analyzed the degradation mechanism of the CH_2O and toluene (C_7H_8) mixture to seek the optimal routes for their decomposition and mineralization. However, the refractory by-products produced by the degradation of photocatalytic gas pollutants under long-term operation would accumulate on the surface of the photocatalyst, blocking the active site and leading to the deactivation of the photocatalyst. The occurrence of photocatalyst deactivation will seriously limit the practical application of photocatalysis technology. Hence, there is still a huge gap between fundamental research and industrial application in this field. The specific aspects of the gap include the design of suitable photocatalysts, the revealing of pollutants degradation mechanisms, the strategies to regulate the reaction pathways, and the development of commercial products for different application scenarios.

Here, we intend to identify this gap and provide a comprehensive review of the recent development of photocatalysis for air purification, including photocatalyst types, reaction pathways of typical air pollutants, and application scenarios (Scheme 1). Firstly, we analyze the published articles on photocatalytic degradation of air pollutants and categorize them based on the types of photocatalytic materials and air pollutants. In addition, photocatalyst reaction mechanisms according to the types of air pollutants, various methods to identify intermediates or by-products, and strategies for regulating reaction pathways are discussed extensively. Subsequently, the application scenarios of photocatalytic air purification are summarized. Lastly, the major challenges for promoting applications of photocatalytic technology are critically discussed and some prospects are delivered.

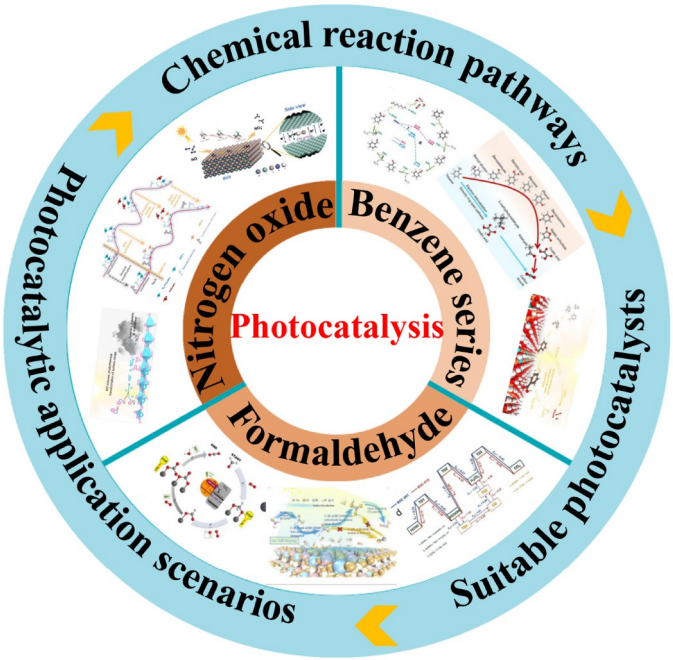

Scheme 1 The structure of the review for photocatalytic purification of typical air pollutants.

Photocatalytic purification of typical air pollutants

Nitrogen oxide (NO_x)

Why is it important?

Among various air pollutants, NO_x is mainly composed of nitric oxide (NO) and nitrogen dioxide (NO_2). In the atmospheric environment, NO is usually in low concentrations but extremely hazardous and can lead to acid rain when it comes in contact with air [32]. Although NO itself is not active, it can be easily oxidized by O_2 in the air to form NO_2, which is a kind of highly corrosive and toxic gas. Meanwhile, photochemical smog, which results from the reaction of NO with other hydrocarbons in the atmosphere, can cause serious harm to human health, and the formation of photochemical smog would be further facilitated with sufficient UV light [33]. Besides, NO can also damage the human respiratory tract, cause methemoglobinemia, and even endanger human life safety [34]. In addition, when NO and VOCs co-exist in the environment and are exposed to sunlight, they can easily interact with each other to produce ozone, thus directly leading to the increase of near-ground ozone concentration [35]. So, how to effectively remove atmospheric NO_x is still a pressing issue to be solved. Currently, the traditional means of purifying NO_x mainly include adsorption, selective catalytic reduction, and thermal catalysis [36]. However, these processes usually require high temperature, high-pressure environments, reducing agents, and even precious metals, such as Ru, Pd, and Pt. Given the harsh conditions, the high energy consumption, and the cost of traditional technologies. It is, therefore, necessary to develop energy-efficient and environmentally friendly NO_x purification technology [37–39]. Photocatalysis, which enables the efficient use of solar energy under mild conditions, has shown great potential in the field of photocatalytic NO_x purification.

What are the chemical reaction pathways?

The reaction pathways involved in photocatalytic purification of NO_x have been widely studied, and the general mechanism is illustrated in Figure 1A. When illuminated with light, photo-electrons (e^-) and holes (h^+) are generated on the surface of the photocatalyst, and then react with small molecules adsorbed on the surface, such as O_2 and H_2O, respectively, to form ROS through the following reaction process.

$$H_2O \rightarrow H^+ + OH^- \quad (1)$$

$$h^+ + OH^- \rightarrow \cdot OH \quad (2)$$

$$e^- + O_2 \rightarrow \cdot O_2^- \quad (3)$$

Subsequently, NO pollutant would be oxidized by ·OH and $\cdot O_2^-$, respectively, and eventually, yield the final product of nitrate via two main intermediates HNO_2 and NO_2 [2].

$$NO + \cdot OH \rightarrow HNO_2 \quad (4)$$

$$HNO_2 + \cdot OH \rightarrow NO_2 + H_2O \quad (5)$$

$$NO_2 + \cdot OH \rightarrow HNO_3 \quad (6)$$

$$NO + \cdot O_2^- \rightarrow NO_3^- \quad (7)$$

$$2NO + \cdot O_2^- + 3e^- \rightarrow 2NO_2 \quad (8)$$

$$3NO_2 + 2 \cdot OH \rightarrow 2NO_3^- + NO + H_2O \quad (9)$$

$$HNO_3 \rightarrow H^+ + NO_3^- \quad (10)$$

In recent years, Dong's group has explored the reaction mechanism of NO oxidation extensively through a combination of *in-situ* DRIFTS and DFT calculations and gained deep insight into the rate-determining step. As shown in Figure 1B, they took g-C_3N_4 as the research model to explore the tune of NO reaction pathways with or without Au decorating [40]. For pristine g-C_3N_4, the processes of $NO \rightarrow NO_2 \rightarrow NO_3^-$ are both energetically unfavorable, resulting in the accumulation of NO_2 on the surface. The dissociation of the O_2 molecule is identified as the rate-determining step. In contrast, NO could be easily oxidized to nitrate by $\cdot O_2^-$ on the surface of Au@g-C_3N_4. These results show that Au as the active center of electron accumulation could effectively reduce the energy barrier, regulate the reaction pathway, inhibit the production of toxic by-products and promote the transformation of NO to final products. The schematic diagram in Figure 1C effectively illustrates the reduction of reaction activation energy and the improvement of photocatalytic efficiency by electron localization [41]. Figure 1D describes the calculated adsorption energy and bond length of several major intermediate adsorption products for g-C_3N_4 and Sr intercalated g-C_3N_4. Different from the above literature, two new intermediates *cis*-N_2O_2 and *trans*-N_2O_2 were detected on the g-C_3N_4 surface with or without Sr doping. For the pristine g-C_3N_4, the reactions of the $NO \rightarrow$*cis*-$N_2O_2 \rightarrow$*trans*-N_2O_2 process are energy favorable. However, further oxidation of *trans*-N_2O_2 requires external energy, which is not conducive to occurring. Surprisingly, all the pathways are exothermic reactions for Sr intercalated g-C_3N_4 and are all energy favorable. Yang *et al.* [43] proposed that the intercalation of -OH groups in BiOI can effectively improve the adsorption and activation of NO, thus reducing the reaction energy barrier and promoting the conversion of NO to NO_3^-, as shown in Figure 1E.

In addition to the adsorption and activation of reactants, the production of ROS and the stability of the final product nitrate are also important indexes to measure photocatalytic efficiency. As shown in Figure 1F, Wang

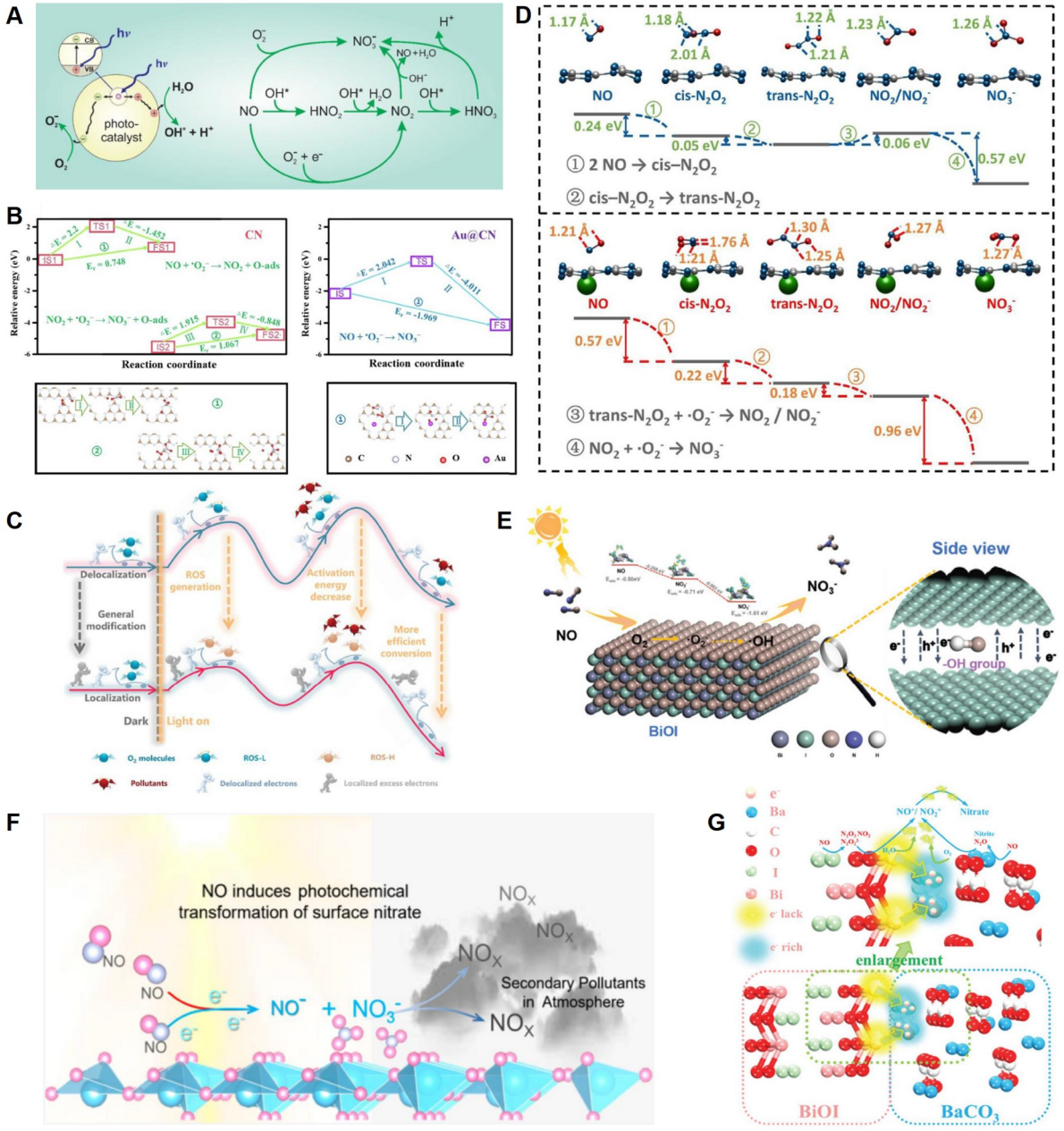

Figure 1 (A) Possible mechanisms of NO_x photocatalytic purification [36]; (B) calculated reaction pathway and structures of initial states, transitional states, and final states for NO photooxidation by $\cdot O_2^-$ on CN and Au@CN [40]; (C) design diagram for localized excess electrons that decrease the reaction activation energies and increase the photocatalysis efficiency [41]; (D) DFT calculated adsorption energy and bond length of several major intermediate adsorption products (upward for CN and downward for Sr intercalated CN), all lengths are given in Å [42]; (E) detailed mechanism of photocatalytic NO oxidation on -OH intercalated BiOI [43]; (F) diagram of the reduction of the surface NO_3^- by NO and e^- [44]; (G) proposed schematic diagram for the separation and transfer of photogenerated carriers and the photocatalytic process over the insulator–semiconductor heterojunction [45].

et al. [44] found that the N-O bond on the surface NO_3^- can be activated by NO molecule due to the overlap of 2p orbitals, and then the NO^-, generated by NO getting an electron, can react with NO_3^- under light irradiation via the following pathway.

$$NO_3^- + NO^- \rightarrow 2NO_2^- \quad (11)$$

Meanwhile, NO^- is the key species that triggers the decomposition NO_3^- on the surface. Figure 1G depicts the photocatalytic process over the insulator–semiconductor heterojunction, which is accompanied by some other intermediates such as NO^+ and NO_2^+. The above results imply that the existing state of the intermediate is easily affected by the surface structure of the photocatalyst, which will further change the reaction path. But how to stabilize the final product NO_3^- on the catalyst surface is still a challenge.

Which are the most suitable photocatalysts?

According to the available literature, we screen photocatalysts suitable for photocatalytic NO purification and divide the most representative photocatalysts into four categories, which are summarized in Table 1. The vast majority of photocatalysts used for NO purification are applicable in visible light. In this way, it is more practical when dealing with low concentration NO in the air.

At present, although a series of efficient catalysts for photocatalytic NO purification have been developed, and the reaction mechanism has been deeply explored through *in-situ* DRIFTS and DFT calculations, there are still many challenges. The photocatalytic NO purification performance lacks a uniform evaluation

Table 1 Summary of various photocatalysts for NO purification

Typical species	Photocatalyst	Light source (light absorption range)	Reaction system	Purification rate (%)	Stability (min)	Reference
Bi-based	Ba/BiOBr	150 W, visible light (≥420 nm)	Continuous flow reaction system	42.0	≥150	[46]
	$BiOI/Bi_2O_2SO_4$	150 W, visible light (≥420 nm)	Continuous flow reaction system	49.6	≥150	[47]
	Ov/Bi_2WO_6	150 W, visible light (≥420 nm)	Continuous flow reaction system	47.0	≥150	[48]
	Bi_2O_3	150 W, visible light (≥420 nm)	Continuous flow reaction system	52.0	≥150	[49]
$g\text{-}C_3N_4$-based	$Au@g\text{-}C_3N_4$	150 W, visible light (≥420 nm)	Continuous flow reaction system	41.0	≥30	[40]
	$MnO_x/g\text{-}C_3N_4$	150 W, visible light (≥420 nm)	Continuous flow reaction system	44.0	≥60	[50]
	$Ca/g\text{-}C_3N_4$	150 W, visible light (≥420 nm)	Continuous flow reaction system	54.8	≥180	[41]
	B-doped $g\text{-}C_3N_4$	150 W, visible light (≥420 nm)	Continuous flow reaction system	41.4	≥30	[51]
	C self-doped g- C_3N_4	150 W, visible light (≥420 nm)	Continuous flow reaction system	56.8	≥150	[52]
TiO_2-based	TiO_2-Ov	visible light (≥420 nm)	Continuous flow reaction system	60.0	≥170	[53]
	$Ag@TiO_2$	300 W, visible light (≥420 nm)	Continuous flow reaction system	63.0	≥250	[54]
Insulator-based	$CaCO_3/g\text{-}C_3N_4$	150 W, visible light (≥420 nm)	Continuous flow reaction system	45.0	≥300	[55]
	$CaSO_4/BiOI$	150 W, visible light (≥420 nm)	Continuous flow reaction system	54.4	≥155	[56]
	Ba-vacancy $BaSO_4$	8 W, UV light (≥254 nm)	Continuous flow reaction system	42.0	≥30	[57]
	$BaCO_3/BiOI$	150 W, visible light (≥420 nm)	Continuous flow reaction system	47.5	≥30	[45]

criterion, which affects the objective evaluation of catalyst performance. In the later stage, it was essential to establish a scientific evaluation system in combination with the actual pollution scene. Besides, it is necessary to further investigate the influence of coexisting molecules such as H_2O, SO_2, O_3, and VOCs in the atmosphere on the photocatalytic purification of NO, and then the photocatalysts with excellent performance should be selected to expand their applicability. The photocatalysts for NO purification reported at this stage only show excellent performance in laboratory research. However, there is still a big gap for practical application. It is necessary to further optimize the synthesis process and loading process of catalysts, systematically evaluate the economic and environmental effects of these photocatalysts and provide technical support for the large-scale application of high-efficiency photocatalytic purification of NO.

Formaldehyde

Why is it important?

Formaldehyde (HCHO), as one of the dominating VOCs emitted from industry activities, consumer products, and furnishing materials, endangers both urban environments and ecological health. Formaldehyde exists both in an indoor environment where the concentration is low and outdoor location where the concentration is high. Due to the mild reaction conditions and the green energy required, photocatalysis technology has been widely utilized for HCHO oxidation removal. However, there are still concerns about low photocatalytic efficiency and secondary pollution caused by toxic by-products. To achieve the overall improvement of photocatalytic HCHO decomposition performance, the binding form and conversion mechanism of HCHO on the photocatalyst surface demand to be revealed.

What are the chemical reaction pathways?

TiO_2-based catalyst is one of the most common photocatalysts used for HCHO degradation. Generous hydroxyl groups are usually present on the surface of TiO_2. Therefore, HCHO is adsorbed on the hydroxyl groups of the catalyst surface via hydrogen bonding, as shown in Figure 2A [58]. In the dry condition, most of the hydroxyl sites on the TiO_2 surface are occupied by HCHO, and the superoxide radicals play an essential role in triggering the HCHO oxidation. In humid conditions, abundant water vapor is introduced to enhance the generation of hydroxyl radicals, resulting in hydroxyl radical dominated HCHO oxidation. The strong oxidizing properties of superoxide and hydroxyl radicals cause the HCHO to be oxidized to the intermediate (formate), followed by the final products (CO_2 and H_2O). The humidity has a positive effect on the photocatalytic oxidation of HCHO because the introduction of water leads to an accumulation of the hydroxyl radicals on the catalyst surface. Therefore, the high degradation rate of formaldehyde in a humid environment can be achieved. Notably, humidity becomes a negative character when the humidity level is above 2000 ppmv. In addition to the effect of moisture, Zhu *et al.* [59] identified the contribution of visible light and proposed new insights into the mechanism for photocatalytic HCHO oxidation over plasmonic Au/TiO_2. As shown in Figure 2B, HCHO undergoes four sequential reaction steps (κ1, κ2, κ3, κ4) with different reaction conditions. At step κ1, HCHO is oxidized to trioxymethylene (DOM). At step κ2, DOM is oxidized to formate. At step κ3, the formate is further oxidized to carbonate. At step κ4, carbonate is decomposed to CO_2 in the presence of moisture. The results of the conditional experiment prove that steps of κ1 and κ2 are

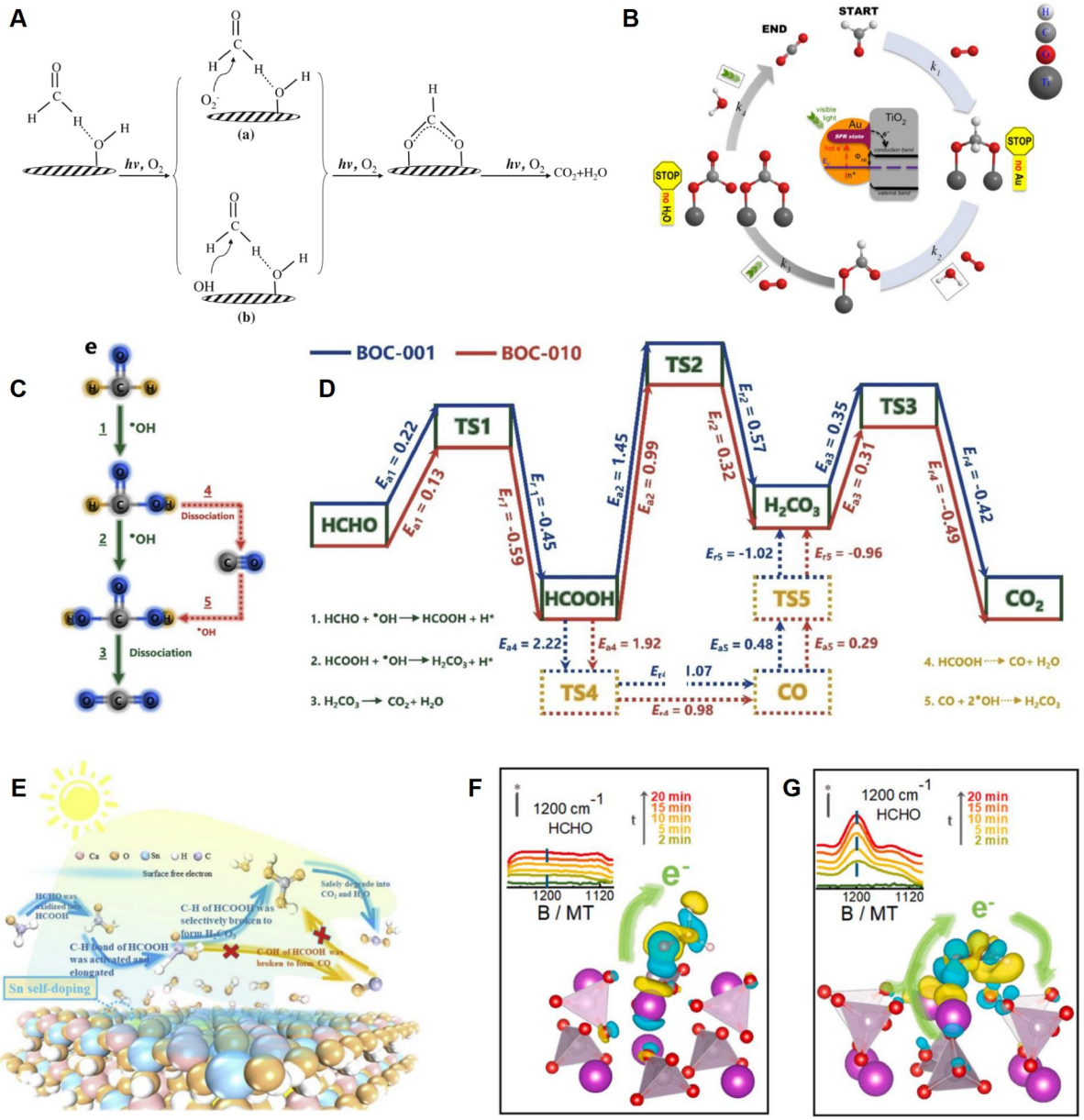

Figure 2 (A) Proposed reaction scheme for the photocatalytic oxidation of formaldehyde on the pure TiO_2: superoxide radicals as the oxidant; hydroxyl radicals as the oxidant [58]; (B) schematic diagram of the proposed pathway for photocatalytic oxidation of formaldehyde over Au/TiO_2 under visible light [59]; (C) schematic illustration for the binary reaction pathways for HCHO degradation [60]; (D) calculated activation energies and reaction energies for the primary and secondary reaction pathways of HCHO degradation, positive and negative depict energy absorption and release respectively [60]; (E) schematic for photocatalytic oxidation of HCHO through selective breakage of C-H in intermediate species (HCOOH) on the surface of Sn self-doped $CaSn(OH)_6$ [61]; the charge difference distribution after HCHO adsorption and the corresponding plot of *in situ* DRIFTS tests for HCHO interaction in the dark on the HBPO (F) and MBOP (G) surface [62].

much faster than κ3 and κ4. The rate-determining steps of the overall reaction are formate oxidation to carbonate (κ3) and carbonate decomposition (κ4). Moisture can accelerate DOM oxidation to formate and is indispensable to carbonate decomposition. Visible light can enhance the rate-determining steps of formate oxidation to carbonate and carbonate decomposition. As a result, the formation rate of intermediates and final products increased significantly.

For the multiple elementary reactions of photocatalytic air purification, the generation of toxic intermediates is a troublesome issue that remains the major hindrance to the advancement of photocatalysts for practical applications. Li *et al.* [60] proposed the particular binary channel reactions in HCHO oxidation, including pathway I of HCHO→HCOOH→H_2CO_3→CO_2 (path 1–3) and pathway II of HCHO→HCOOH→CO→H_2CO_3→CO_2 (path 1, 4, and 5) (Figure 2C). The HCOOH oxidation is the rate-determining step (Figure 2D). Hence, the HCHO degradation efficiency is directly related to the activation energy of HCOOH transformation. However, CO plays a disgusting role as the secondary pollutant during photocatalytic HCHO oxidation. To realize safe and efficient photocatalytic HCHO oxidation, Wang *et al.* [61] constructed the photocatalyst surface with abundant free electrons distribution to realize the selective breakage of C-H bonds in HCOOH formed as the intermediate of HCHO oxidation (Figure 2E). Therefore, the reaction pathway can be altered to avoid the generation of toxic by-products (CO). Additionally, the controlling of surface atomic arrangement can modulate the adsorption model of HCHO from single-point to bridging. The efficient conversion of intermediate (HCOOH*) can be facilitated while suppressing CO generation (Figure 2F and 2G) [62].

The above results show that the degradation pathways and rate-determining steps of photocatalytic HCHO oxidation have been relatively clearly revealed, which is attributed to the fact that HCHO is a simple small molecule. The key intermediate, HCOOH, is the dominant driver during the HCHO degradation. By tailoring the electronic structure of the photocatalyst surface and the adsorption configuration of the reactants, the reaction pathway can be effectively regulated. However, most of the state-of-the-art structure-activity relationships of photocatalytic HCHO degradation are still established under the condition of ultraviolet light (UV). It is urgent to achieve continuous and efficient visible-light degradation of HCHO. In addition to optimizing the reaction conditions, such as humidity, light intensity, and residence time, developing photocatalysts with a more positive valence band and visible light response may be a more effective method. As a C1 feedstock and reaction intermediate for CO_2 reduction, the HCHO can be reused to produce value-added chemicals, such as photocatalytic reduction of HCHO to CH_4 fuels.

Which are the most suitable photocatalysts?

There have been numerous studies with a variety of photocatalysts in photocatalytic HCHO degradation, which are summarized in Table 2. At present, getting the photocatalytic purification of HCHO to CO_2 and H_2O at ambient temperature exhibits the advantages of no energy consumption, complete purification, no secondary pollution, and high removal efficiency, which is the mainstream development direction of HCHO photocatalytic purification. However, most of the catalysts with the above capabilities are noble metal-based catalysts or precious metals as active additives. It is generally known that precious metals on the earth are rare and expensive. Therefore, the development of non-noble metal-based photocatalysts for photocatalytic purification of HCHO at ambient temperature is an important research goal in the future.

Benzene series

Why is it important?

The benzene series represent the main typical VOCs emitted in the air and result in high health risks due to its

Table 2 Summary of various photocatalysts for HCHO oxidation

Photocatalyst	Light source (light absorption range)	Reaction system	Degradation efficiency (%)	Stability (min)	Reference
BiOCl-010	125 W, UV light (≥350 nm)	Continuous flow reaction system	45.0	≥180	[60]
Sn-$CaSn(OH)_6$	300 W, UV lamp (≥330 nm)	Continuous flow reaction system	79.3	≥60	[61]
Monoclinic $BiPO_4$	300 W, UV lamp (≥275 nm)	Continuous flow reaction system	79.8	≥245	[62]
TiO_2@NH_2-MIL-125	125 W, UV irradiation (≥500 nm)	Continuous flow reaction system	90.0	≥45	[63]
Na/g-C_3N_4	250 W, metal halide lamp (≥410 nm)		75.0	≥400	[64]
H-TiO_2@graphene	300 W, Xe lamp, UV irradiation (≥440 nm)	Static reactor	92.0	≥840	[65]
$BiSbO_4$-200	300 W, mercury lamp (≥400 nm)	Continuous flow reaction system	92.0	≥200	[66]

inherent chemical toxicity. They are relatively difficult to be decomposed because of the stable benzene ring. The co-existence of VOCs and NO_x in the atmosphere would promote the generation of ozone via photochemical processes. For complete mineralization of VOCs with rings, the ring-opening reaction is regarded as the rate-determining step which should be fully considered when designing catalysts. Required by the demand for sustainable development, effective and eco-friendly technology is desired for VOCs removal. Photocatalytic oxidation is a promising purification technology, especially for the degradation of benzene series, due to its strong oxidation capacity at room temperature and atmospheric pressure.

What are the chemical reaction pathways?

During photocatalytic toluene degradation, there are two main different reaction pathways, including (Pathway I) hydrogen abstraction and (Pathway II) OH addition (Figure 3A) [67]. In pathway I, the oxidation takes place on the side chain of the methyl group. The reaction mechanism could probably follow the scheme: toluene→benzyl alcohol→benzaldehyde→benzoic acid. For pathway II, •OH could attack the aromatic ring to replace the aromatic hydrogen. The possible reaction scheme is presented as follows: toluene→cresol→hydroquinone or methyl-*p*-benzoquinone. Subsequently, these intermediates of two reaction pathways could further convert to benzoquinone. With further oxidation, the aromatic ring is broken, and all the intermediate products are oxidized to form CO_2 and H_2O with enough oxidizing radicals. The intermediate products are different for the two pathways. Besides, the pathway I is believed to be the primary reaction path for toluene degradation because the weakest bond in the toluene molecule is the C-H bond of the methyl group. By calculating the primary reaction pathways in photocatalytic toluene decomposition, as shown in Figure 3B, no energy barriers are found for the benzyl oxidation part (steps 1–3), indicating that toluene can be favorably converted to ring-containing intermediates (benzyl alcohol, benzaldehyde, and benzoic acid) [68]. However, for complete mineralization of toluene, the ring-opening pathway of the benzene ring in these intermediates becomes the rate-determining steps (4–7). Fortunately, low activation energies are required for the ring-opening reaction at benzaldehyde and benzoic acid. It is worth noting that the lowest energy barrier is the ring-opening starting from benzoic acid. These results indicate that a more efficient ring-opening reaction can be realized as the benzyl gets fully oxidized to benzoic acid. Accordingly, as shown in Figure

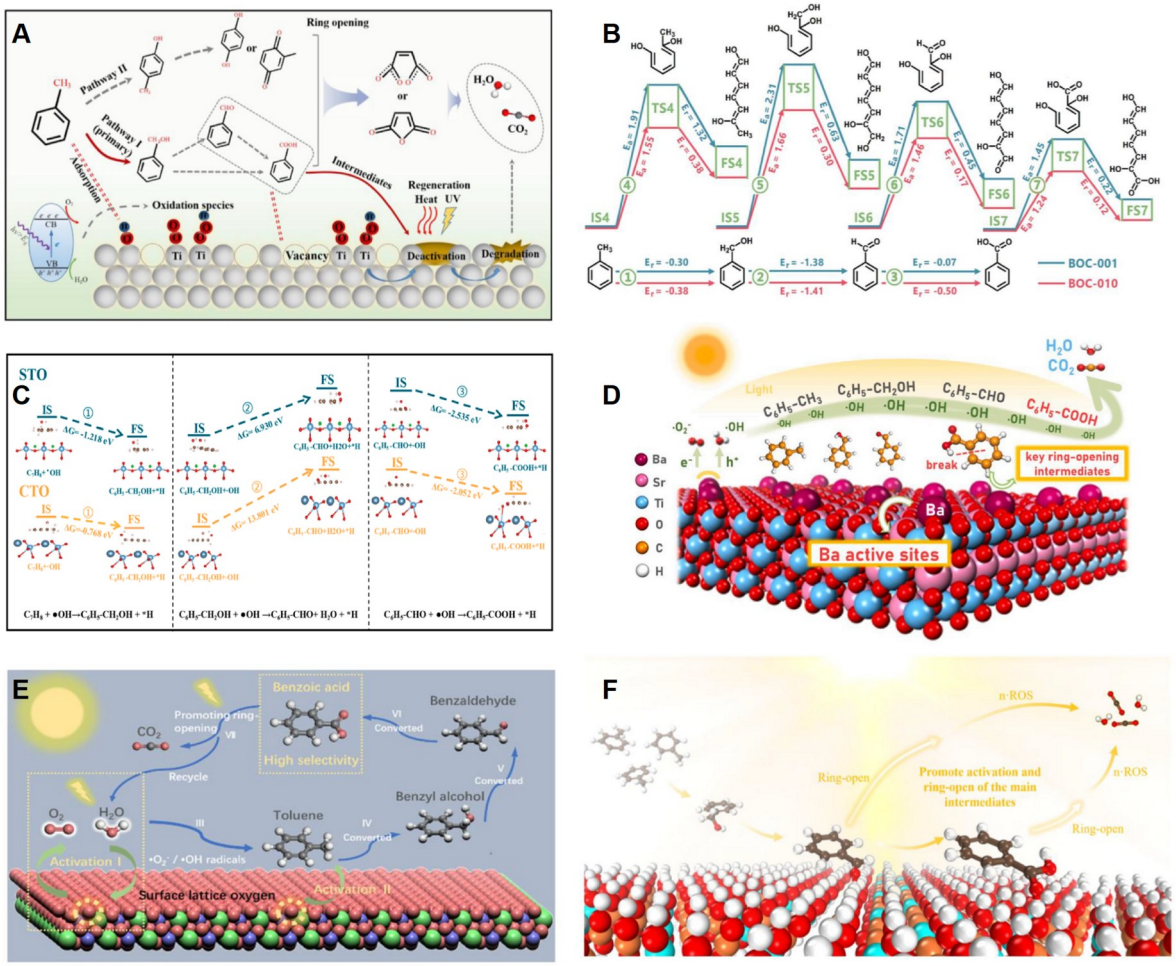

Figure 3 (A) Possible reaction mechanisms of toluene degradation and catalyst regeneration [67]; (B) the calculated reaction coordinates for benzyl oxidation (path 1–3) and aromatic ring-opening (path 4–7) [68]; (C) free energy of conversion processes of toluene to benzoic acid via the route of toluene→benzyl alcohol→benzaldehyde→benzoic acid on STO and CTO, IS (initial state), FS (final state) [69]; (D) illustration of the role of Ba active sites in photocatalytic toluene decomposition on SBTO [70]; (E) illustration of the viral effect for lattice oxygen activation in photocatalytic toluene decomposition on $Sr_2Sb_2O_7$ [71]; (F) schematic for photocatalytic oxidation of toluene over ZT-LDH [72].

3C, the overall decreased reaction energy on the $SrTiO_3$ surface during the toluene oxidation path realizes the highly selective formation of intermediate (benzoic acid) to accelerate the ring-opening and mineralization process of photocatalytic toluene degradation [69].

In addition, the establishment of active sites on the photocatalyst surface is the critical factor to achieve highly selective benzyl oxidation. As shown in Figure 3D, the local electronic center constructed at Ba active sites intensifies the charge transfer between catalyst surface and adsorbed molecules [70]. The strong oxidative species generated by enhanced activation facilitate the selective conversion of toluene to generate benzoic acid. Consequently, the photocatalyst displays the efficient degradation and stable mineralization of photocatalytic toluene. For metal oxide, the activated lattice oxygen on the photocatalyst surface is favorable for adsorption and activation of toluene and intermediates and then realizes the selective conversion of benzoic acid (Figure 3E) [71]. Interestingly, CO_2 desorption and lattice oxygen reactivation through H_2O

avoid the competitive adsorption between final products and specific intermediates. Additionally, as shown in Figure 3F, the hydrogen atoms on the hydroxyl groups in the LDH can selectively attract the oxygen atoms in the C=O bond of benzaldehyde and benzoic acid, thereby improving the selectivity of photocatalysis and reducing the generation of toxic by-products [72].

Although the highly selective oxidation of methyl group to benzoic acid facilitates efficient photocatalytic toluene degradation, some intermediates in pathway I (toluene→benzyl alcohol→benzaldehyde→benzoic acid) are also easy to cause the deactivation of the photocatalyst with poor oxidation ability. This dramatically diminishes the commercial value of photocatalysis as a practical flue gas purification technology. Hence, the intrinsic reason for the deactivation of the photocatalyst is revealed to provide a new theoretical reference to design efficient and stable photocatalysts for toluene degradation. Chen *et al.* [73] found that a considerable accumulation of benzaldehyde and weak ability of ring-opening on P25 are the direct causes of deactivation. The vast accumulation of benzaldehyde and benzoic acid on the catalyst surface blocks the active sites and causes a decrease in photocatalytic efficiency. Differently, on the surface of Ga_2O_3, adsorbed intermediates quickly and easily open the aromatic ring and further mineralize into small inorganic molecules (Figure 4A). The different ring-opening abilities of intermediates on the surface Ga_2O_3 and P25 decide their durability differences during prolonged toluene degradation. Alternatively, a direct and effective method is to modulate the reaction pathway to avoid the generation of benzoic acid on the photocatalyst surface. As shown in Figure 4B, the benzaldehyde was unlikely converted to benzoic acid on the $In(OH)_3$ (IO) catalyst surface due to the presence of thermodynamic energy barriers [74]. Hence, the benzaldehyde was unlikely converted to benzoic acid on the IO catalyst. More efficiently, the aromatic ring can be directly opened, which is observed over the modified boron carbonitride photocatalyst (BCN-C) [75]. As shown in Figure 4C, this could bring out a more efficient and concise ring-opening pathway, producing fewer carbonaceous intermediates. The delocalized electrons on the photocatalyst surface are essential to enable the direct ring-opening of the aromatic ring. The strong oxidation ability of •OH generated over BCN-C and enhanced the interaction between the reactants and the catalyst made it possess the ability to attack the aromatic ring of toluene directly. Hence, BCN-C exhibits remarkable durability, a high mineralization rate, and immensely enhanced photocatalytic degradation performance.

In order to improve the ring-opening efficiency of the benzene ring, except for the abovementioned interaction of toluene with different photocatalyst surfaces, changes in the groups on the benzene ring play a vital role in the ring-opening. The intrinsic relationship between the methyl number and ring-opening reaction efficiency is worthy of investigation. As shown in Figure 4D, the methyl number on the benzene ring was dominantly responsible for the elevated ring-opening and decomposition efficiency [76]. The introduction of methyl groups greatly influences the distribution of electrons on the phenyl ring, which enhances charge transfer and reduces the stability of the conjugated π bond. Therefore, the introduction of carbon-containing groups on the benzene ring can effectively activate the benzene ring and reduce the ring-opening energy barrier of the reaction. Additionally, during the photocatalytic mixed degradation reaction of HCHO and toluene, the addition of HCHO into toluene leads to the generation of *o*-tolualdehyde as key intermediates (Figure 4F), which can elevate the adsorption and activation of the aromatic ring [31]. Compared with the vital intermediate (*o*-methylphenol) of OH addition at the aromatic ring of toluene (Figure 4E), the reaction energy for HCHO addition is lower than that of OH addition (Figure 4G). Besides, the addition of HCHO on toluene efficiently decreases the Gibbs free energy for enhanced ring-opening.

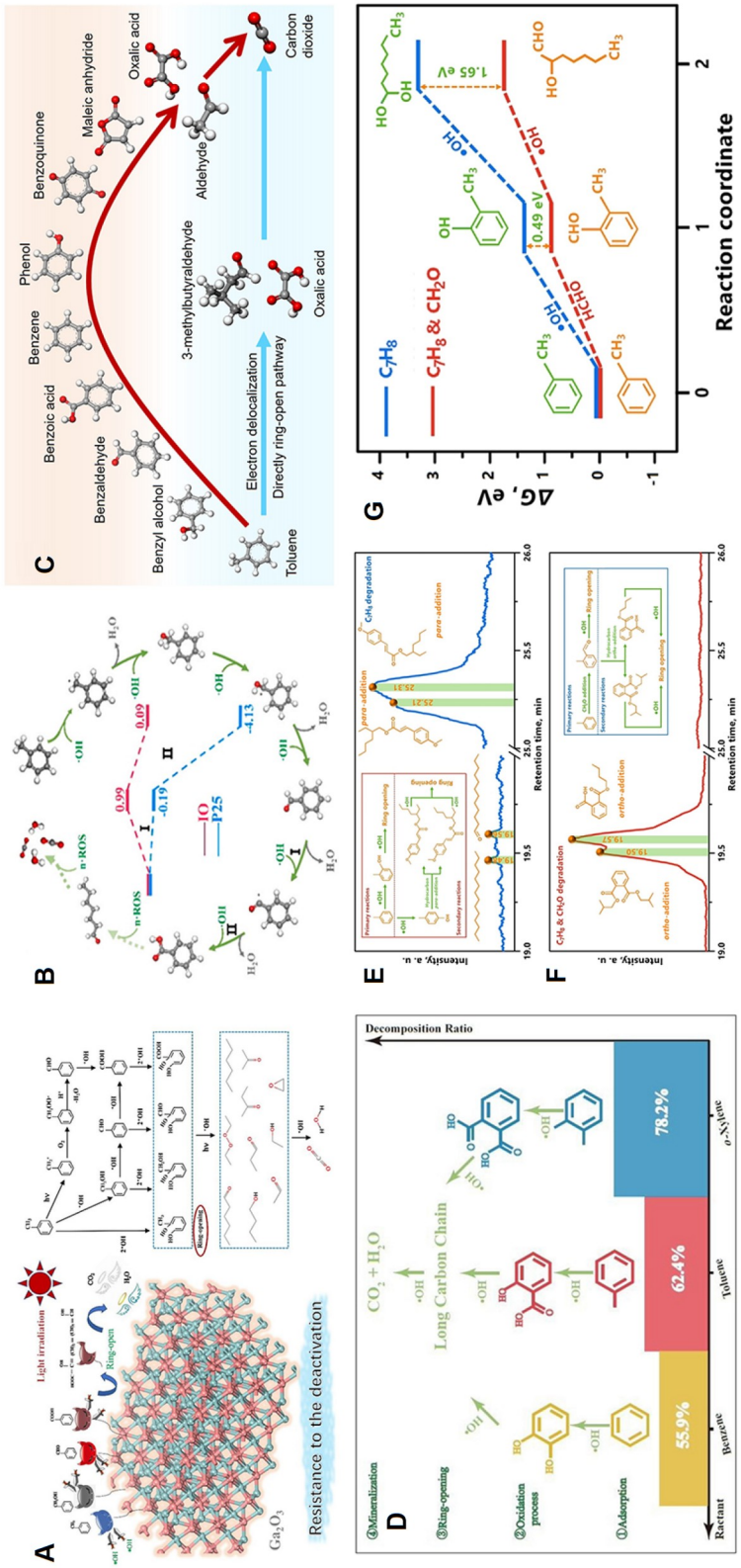

Figure 4 (A) The intermediate speciation and chemistry of the photocatalytic toluene oxidation on 120-β-Ga_2O_3 [73]; (B) proposed C7 conversion pathway and calculated reaction energies of hydroxyl induced toluene photooxidation on catalysts [74]; (C) schematic illustration for different paths of photocatalytic gas toluene degradation [75]; (D) the illustration of roles of methyl number on mechanisms and performance of photocatalytic decomposition of benzene, toluene, and *o*-xylene [76]. GC-MS chromatogram for the determination of reaction intermediates in the gas-phase photocatalytic decomposition of toluene: as a single individual component (E) and as part of a mixture of CH_2O and C_7H_8 (F) [31]; (G) diagram of Gibbs free energy variation on the SnO_2 surface [31].

The above investigations indicate that breaking the stability of benzene ring is a key factor to realize efficient photocatalytic mineralization, including the direct addition of strong •OH radicals, selective generation of benzoic acid with lower ring-opening energy barriers, or synergistic addition between mixed pollutants. Since the toluene oxidation process involves a variety of complex intermediates, the results of the ring-opening pathways of benzene ring studied above are mostly derived from theoretical simulations. To reveal the reaction mechanism more accurately, direct experimental evidence remains to be provided in terms of *in-situ* formed reactive species and intermediates with high resolution. Isotopic labeling of O_2 or H_2O molecules combined with *in situ* infrared spectroscopy would be an advanced characterization tool to track the molecular conversion processes.

Which are the most suitable photocatalysts?

There have been numerous studies with a variety of photocatalysts applied in toluene degradation, which are summarized in Table 3. Photocatalytic technology can degrade toluene to CO_2 and H_2O at room temperature. However, some toxic by-products may inevitably be formed in this process. Therefore, it is necessary to develop more efficient photocatalysts. At present, doping, crystal surface regulation, or heterojunction construction are effective means to overcome the inherent limitations of photocatalysts and improve the photocatalytic activity under visible light. Meanwhile, the electron and hole recombination can be effectively suppressed. In addition, it is essential to explore the doping amount and the proportion of components in the heterojunction.

Various photocatalytic application scenarios

The main challenges for practical application of photocatalytic air purification are (1) mass transfer, (2)

Table 3 Summary of various photocatalysts for toluene oxidation

Photocatalyst	Light source (light absorption range)	Reaction system	Degradation efficiency (%)	Stability (min)	Reference
Cu_2O NWs/Cu mesh	300 W, xenon lamp	Static reactor	99.9	≥1200	[77]
β-Ga_2O_3	300 W, mercury lamp (≥280 nm)	Continuous flow reaction system	77.3	≥300	[73]
BiOCl-010	300 W, UV light (≥350 nm)	Continuous flow reaction system	61.0	≥30	[68]
$Sr_{1-x}Ba_xTiO_3$	300 W, high-pressure mercury lamp (≥340 nm)	Continuous flow reaction system	73.94	≥180	[70]
$SrTiO_3$	300 W, mercury lamp (≥390 nm)	Continuous flow reaction system	80.0	≥70	[69]
$Sr_2Sb_2O_7$	300 W, high-pressure Hg lamp (≥300 nm)	Continuous flow reaction system	73.3	≥420	[71]
Zn-Ti-LDHs	300 W, mercury lamp (≥340 nm)	Continuous flow reaction system	75.2	≥180	[72]
$In(OH)_3$	300 W, UV mercury lamp (≥245 nm)	Continuous flow reaction system	57.7	≥180	[74]
SnO_2	125 W, mercury lamp (≥360 nm)	Continuous stream reaction system	62.4	≥150	[76]
LDH/Zn_2SnO_4	UV light, high-pressure mercury lamp (≥240 nm)	Continuous flow reaction system	89.8	≥300	[78]

durability and deactivation, (3) utilization of photons, (4) catalyst adhesion to substrates, (5) by-product generation and its adverse health consequences [79]. Achieving high-efficiency long-term stability is an important goal for the commercialization of photocatalytic applications.

Application in indoor air purification

NO_x and VOCs released by furniture and building materials will seriously affect indoor air quality, including NO, NO_2, benzene, toluene, polycyclic aromatic hydrocarbons (especially benzo[a]pyrene), trichloroethylene, perchloroethylene, and formaldehyde. Compared with the outdoor environment, the level of indoor air pollutants can reach higher values. The concentration of indoor NO_2 is between 15 and 200 ppb (1 ppb=1 μg L^{-1}). While in industrial workplaces and gas stove equipment, NO_2 concentration may reach 1–2 ppm (1 ppm=1 mg L^{-1}) [80]. For the treatment of indoor pollutants by photocatalytic technology, laying photocatalytic tile is an effective strategy for indoor air purification. As shown in Figure 5A, Jiang *et al.* [81] coated the N, F, and Fe ion triple-doped TiO_2 photocatalytic function layer on tiles for removing NO air pollutants and organic compounds in the indoor and outdoor air under visible light. In addition to improving air quality, the modified ceramic tile also possesses low water absorption, good fastness, and antibacterial ability to reduce the risk of bacterial infection. Therefore, photocatalytic tile is a promising candidate for practical application in indoor and outdoor environment improvement.

Long-term exposure to indoor VOCs may greatly increase the risks of allergy, respiratory illness, and even

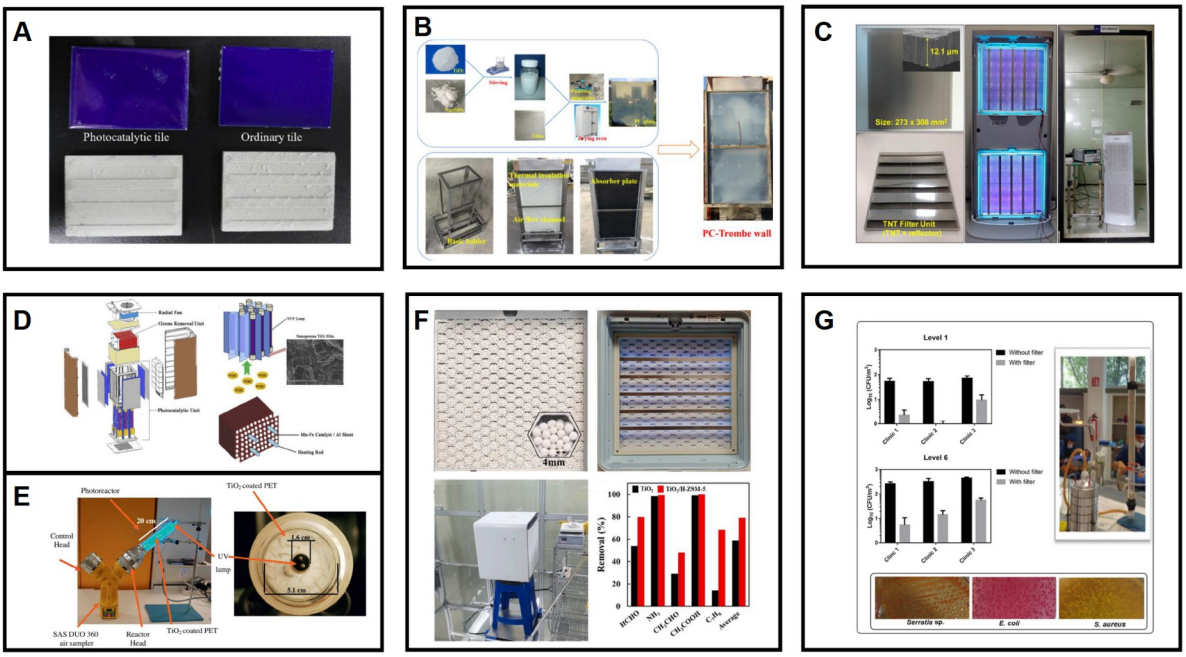

Figure 5 (A) Photocatalytic and ordinary tiles [81]; (B) manufacturing and assembling processes of PC-Trombe wall system [82]; (C) an air cleaner (AX7000, Samsung) equipped with two 001-TNT filter units and 30 UV-LEDs (Seoul Viosys, CUN66A1B) [25]; (D) schematic diagrams of the VUV-PCO air purifier [83]; (E) photocatalytic reactor of biological sampling system (left) and reactor frontal view (right) [84]; (F) a test chamber (8 m^3) with the air purifier for VOC removal experiments [85]; (G) schematic representation of the photocatalytic air purifier prototype [86].

cancer. Using light energy can not only purify the VOCs in the air but also adjust the indoor temperature. Yu *et al.* [82] constructed a new type of solar gradient photocatalysis-Trombe wall system (Figure 5B), which can achieve the dual functions of space heating and removal of indoor formaldehyde. Under solar radiation, photocatalytic oxidation of formaldehyde is activated by ultraviolet light, and the remaining visible and infrared light is collected to heat the indoor environment. The daily clean air and formaldehyde degradations are 164.0 $m^3/(m^2$ day) and 100.0 mg/(m^2 day), respectively. It is estimated that the initial investment of the photocatalysis-Trombe wall system will be recovered in about 12 years. The indoor air purifier can improve the air environment quickly and efficiently, and has been sought after and loved by many families in recent years, owing to its small and convenient characteristics. Through a new method that is easy to scale up, Weon *et al.* [25] synthesized (001)-surface exposed TiO_2 nanotubes (001-TNT) and was successfully amplified and installed on a commercial air purifier, as seen in Figure 5C. The air purifier achieves an average VOC removal efficiency of 72.0% (running for 30 min) in an 8 m^3 laboratory, meeting the air purifier standard agreement. Xu *et al.* [83] have constructed an innovative vacuum ultraviolet photocatalytic oxidation (VUV-PCO) air purifier (Figure 5D), which simultaneously eliminates VOC and O_3 in a closed real room for the first time. The air purifier has a high removal efficiency of formaldehyde, and considerable removal efficiency of benzene, toluene, *m*-xylene, *o*-xylene, valeraldehyde, octanal, and nonanal. The air purifier showed good stability during the removal of formaldehyde decomposition and TVOC during the intermittent three-time on/off operation. The ozone content was reduced by 70% when the device was heated. Efficient portable air purifiers are expected to be a potential method for indoor air quality improvement, due to their small size and low price.

As active components of air pollution particulate matter, bacteria, fungi, and viruses cannot be ignored for indoor air quality and safety control. As shown in Figure 5F, a practical-grade photocatalytic air purifier equipped with a TiO_2/H-ZSM-5 composite bead filter was established by Kim *et al.* [85], which is proved to effectively remove indoor VOC and viruses under UVA-LED lighting. The photocatalytic air purifier can effectively remove the atomized virus particles of the bacteriophage Phi-X 174. More than 99.999% of the viral RNA of SARS-CoV-2 is removed within 1 h, eliminating the infectivity of the virus. The air purifiers equipped with composite bead filters are ready for practical applications in homes and hospitals. Sánchez *et al.* [84] propose that the monolithic transparent polymer coated with a sol-gel TiO_2 film was used to treat real indoor air in a laboratory-scale single-step annular photocatalytic reactor (Figure 5E). The photocatalytic reactor can realize disinfection and sterilization while eliminating indoor VOC. Martínez-Montelongo *et al.* [86] has prepared TiO_2-Cu^{2+}@perlite and Ag@TiO_2-Cu^{2+}/perlite supported materials. A prototype of a photocatalytic air purifier was constructed with novel materials (Figure 5G), showing a better air disinfection activity at lower doses. The growth inhibition of Gram-negative and Gram-positive bacteria reached up to 99.0%. In addition to eliminating indoor chemical pollutants, disinfection and sterilization of indoor air through portable air purifiers is also a crucial way to improve indoor air quality.

Application in outdoor air purification

In the case of outdoor air purification by photocatalysis, there are some differences compared to indoor air purification, such as the irradiation source, the type of contaminants, and the operation conditions [87]. For outdoor air purification, solar light can be used as the driving force to initiate photocatalytic reactions. The

main target air pollutant from outdoor is nitric oxides which come from automobile exhaust, rather than VOCs. The formed nitrates can be simply washed off with rainwater, and the photocatalyst is thereby self-regenerated without additional treatment [88]. Moreover, outdoor applications are exposed to a harsh environment. The applications are required to withstand high shear rates.

The practical outdoor applications focus on utilizing construction materials with a large surface area that can serve as platforms for photocatalytic air decontamination, like canyon streets, tunnels, bridges, car garages, public outdoor furniture, and external surfaces of buildings [89]. Photocatalysts can be incorporated into building materials (plaster, mortar, paint, or cement) and applied in various forms. Anything made of concrete has the potential for photocatalytic air purification.

TiO_2 is the most popular photocatalyst incorporated in concrete. Meng Chen and co-workers conducted a series of real-scale applications on the road. They utilized permeability technology to immobilize TiO_2 on the surface of porous asphalt roads for the removal of NO_x from vehicle emissions [90]. The purifying rate of vehicle pollutants ranged from 6.0% to 12.0% in the actual outdoor road traffic environment, showing a good environment purification function. As shown in Figure 6A, another study used a TiO_2 and activated carbon permeable spray solution to coat concrete roads, aiming at the degradation of NO_x [91]. High purification efficiency, self-regeneration ability, and good repetition performance were achieved. In addition, they found that the photocatalytic purification of NO_x was related to light intensity and temperature. The reaction rate increased as the light intensity increased, while the reaction rate decreased as temperature increased. Guerrini [92] reported the NO_x levels of the "Umberto I" tunnel in Italy before and after the renovation work by the photocatalytic treatment (Figure 6B). A NO_x reduction of about 20.0% was calculated in the center of the

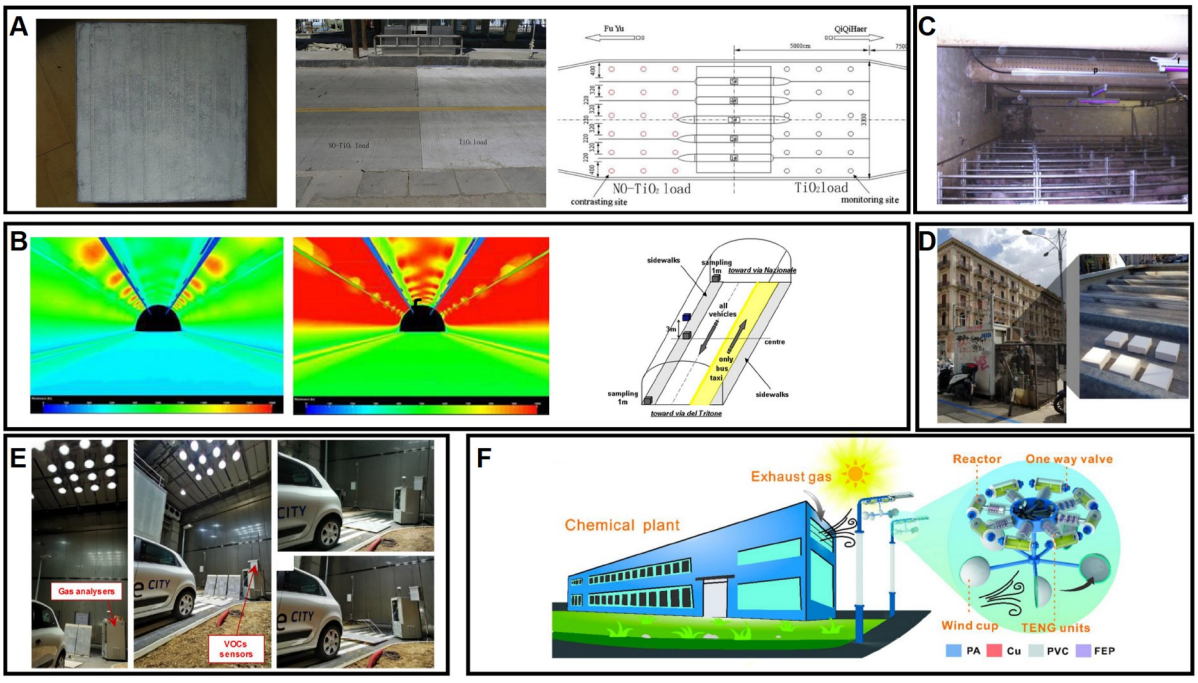

Figure 6 (A) Photocatalytic Nano-TiO_2 on concrete road [91]; (B) simulation design of lighting system in the tunnel [92]; (C) treated swine weaning unit [93]; (D) samples exposed on the top of the Bari Cavour meteoclimatic station in the city centre [94]; (E) sense-city experimental campaign pictures [95]; (F) application scenario of the self-powered photocatalytic degradation system [96].

tunnel as an absolute comparison between the two periods. The photocatalytic paint exhibited an efficient abatement of pollutants in the tunnel vault. Costa *et al.* [93] applied TiO_2-based photocatalytic paint in a swine weaning unit and examined the concentrations and emissions of pollutants (NH_3, CH_4, CO_2, N_2O, and PM_{10}) (Figure 6C). The photocatalytic treatment has beneficial effects on significant decreases in methane concentration (ca. 27.0%, $P<0.05$) and particulate matter emission (ca. 17.0%, $P<0.01$) in swine husbandry with respect to reference one. The limestone surfaces coated with water dispersed TiO_2 nanoparticles were exposed to an urban site for one year to investigate the photocatalytic performance (Figure 6D) [94]. The obtained surface through TiO_2 coating showed better preservation of the surface color early after exposure. But the self-cleaning efficiency was reduced to negligible after eight months due to TiO_2 loss and deactivation.

Other photocatalysts have also been studied for practical application. Le Pivert *et al.* [95] developed construction materials functionalized by low-cost hydrothermal direct growth of ZnO. Bitumen road was produced to evaluate the photocatalytic activity of simultaneous removal of various pollutants from a real car exhaust (O_3, CO_x, NO_x, VOCs) (Figure 6E). All car exhaust components showed a downward trend in the presence of ZnO. Fu *et al.* [96] built a piston-based triboelectric nanogenerator (P-TENG) to enhance gaseous acetaldehyde photocatalytic degradation as shown in Figure 6F. The photocatalyst NH_2-MIL-125 (Ti) was evenly distributed on a conductive substrate which is connected to a P-TENG. The P-TENG can convert wind energy into electrical energy and induce an electric field that could generate more radicals and holes. The photocatalytic removal rate of the system reached 63.0% within 30 min.

Incorporating photocatalyst with construction material is a workable way to scale up the application of photocatalytic air purification. But big challenges remain and wait to be solved, such as the long-term stability, durability under harsh weather and environment, the corrosion of buildings, and the replacement of photocatalysts. Due to the complexity of the application environment, the outdoor application faces more difficulties than the indoor application.

The bottleneck of practical application

Currently, photocatalytic air purification technology has been developed for decades, and photocatalyst technology has been applied in indoor and outdoor air purification. However, the actual application effect is not ideal. There are still few research achievements to realize the industrialization and application, which has become a major scientific problem faced by all mankind. Fundamentally, there are three major bottlenecks.

(1) Low photocatalytic efficiency. Photocatalytic efficiency is one of the important indexes to evaluate the performance of a catalyst. High photocatalytic efficiency can completely degrade organic pollutants in a short time and effectively alleviate environmental pollution. Meanwhile, the high-efficiency photocatalysts can also achieve better purification of air pollution in a small amount. However, most photocatalysts exhibit high photocatalytic activity only under UV light but low activity with visible-light irradiation, such as commercial photocatalyst P25, while the UV light only accounts for about 5% of the sunlight. Therefore, the light absorption efficiency of commercial photocatalysts under sunlight is very low, which leads to low photocatalytic efficiency and limited practical application effect. However, if the catalytic material can display high catalytic activity under visible light, the efficient catalytic purification of air pollutants under LED lights can be realized, so as to effectively solve the problem of air pollution.

(2) Difficult realization of industrial production. In the actual scale-up production process, the preparation conditions are not as controllable and stable as the laboratory conditions, there are many uncontrollable factors, and the problems of cost, energy consumption, environmental protection, stability, and so on need to be considered. Therefore, the development of a feasible and stable preparation method is the key to realizing the industrialized application of photocatalysts.

(3) The loading of powder photocatalyst. Although a great deal of work has been done on the basic research of photocatalysis, there is still a gap between laboratory and industrial applications. For example, the commercialized P25, as a benchmark for evaluating the performance of catalysts, shows a stable photocatalytic purification capacity in photocatalysis, which has also realized mass industrial production. However, the powder photocatalyst is easy to be blown out in the reaction process, which greatly affects the air purification efficiency of P25 and its practical application effect. Therefore, the additional process needs to be carried out, such as the loading of powder photocatalysis, and then pay a lot of cost and energy. This is the gap between material properties and industrial applications.

Conclusions and perspectives

This review summarizes recent advances in photocatalytic purification of typical air pollutants, including NO_x, HCHO, and benzene series. The insights into the mechanisms of pollutant conversion have been discussed extensively for the design of efficient and safe photocatalytic systems. Additionally, the applications of photocatalytic air purification technology indoors and outdoors have gradually set the tone for its contribution to the future of environmental remediation and human health. However, the photocatalytic air pollutant purification process is complicated and the applied research in this field is still limited. There are still major challenges that need to be further investigated.

(1) Even though some intermediates have been observed, more solid experimental evidence should be provided regarding their transient intermediates, especially for the photocatalytic degradation of multiple gaseous pollutants, which is more in line with the practical application. The combination of isotope labeling and *in situ* characterization techniques is essential for identifying reactant migration and transformation on the photocatalyst surface. Besides, the antagonistic or synergistic effects between multiple pollutants and the generation of harmful by-products (e.g., ozone) during photocatalytic degradation should also be further revealed.

(2) The stability of photocatalysts deserves to be taken seriously. The development of deactivation-resistant photocatalysts based on mechanistic understanding is a feasible strategy. Alternatively, the design of a coupled reactor to regenerate the photocatalyst or cover the photocatalyst surface with a porous protective layer may be an effective method.

(3) For outdoor air purification, it is necessary to develop high-performance visible-light-driven photocatalysts to make full use of sunlight, and a balance between visible light absorption efficiency and oxidation capacity is required to achieve continuous and efficient degradation of outdoor air pollution.

(4) For indoor air purification, there are many efficient photocatalysts available. Future work should be focused on the design of reactor structure, systematically considering the relationship among factors such as light, mass transfer, heat transfer, and reaction.

(5) The reuse of typical air pollutants is also worth considering, which can provide a more valuable alternative to conventional environmental governance. The tunable oxidation and reduction capability of photocatalytic technology are expected to enable the targeted conversion of air pollutants to valuable fuels or chemicals.

Funding

This work was supported by the National Natural Science Foundation of China (22176029, 21822601) and Excellent Youth Foundation of Sichuan Province in China (2021JDJQ0006).

Conflict of interest

The authors declare that there are no conflicts of interest to disclose.

References

1 He C, Cheng J, Zhang X, *et al.* Recent advances in the catalytic oxidation of volatile organic compounds: a review based on pollutant sorts and sources. *Chem Rev* 2019; **119**: 4471–4568.

2 Chen R, Li J, Wang H, *et al.* Photocatalytic reaction mechanisms at a gas–solid interface for typical air pollutant decomposition. *J Mater Chem A* 2021; **9**: 20184–20210.

3 Shah V, Jacob DJ, Li K, *et al.* Effect of changing NO_x lifetime on the seasonality and long-term trends of satellite-observed tropospheric NO_2 columns over China. *Atmos Chem Phys* 2020; **20**: 1483–1495.

4 Wang J, Li J, Ye J, *et al.* Fast sulfate formation from oxidation of SO_2 by NO_2 and HONO observed in Beijing haze. *Nat Commun* 2020; **11**: 2844.

5 Nazaroff WW, Goldstein AH. Indoor chemistry: research opportunities and challenges. *Indoor Air* 2015; **25**: 357–361.

6 Liu B, Zhang M, Yang J, *et al.* Efficient ozone decomposition over bifunctional Co_3Mn-layered double hydroxide with strong electronic interaction. *Chin Chem Lett* 2022; **33**: 4679–4682.

7 Gulia S, Shiva Nagendra SM, Khare M, *et al.* Urban air quality management-a review. *Atmos Pollution Res* 2015; **6**: 286–304.

8 Jiang Z, McDonald BC, Worden H, *et al.* Unexpected slowdown of US pollutant emission reduction in the past decade. *Proc Natl Acad Sci USA* 2018; **115**: 5099–5104.

9 Salthammer T, Mentese S, Marutzky R. Formaldehyde in the Indoor Environment. *Chem Rev* 2010; **110**: 2536–2572.

10 Zhu T. Air pollution in China: scientific challenges and policy implications. *Natl Sci Rev* 2017; **4**: 800.

11 Srivastava A, Joseph AE, Patil S, *et al.* Air toxics in ambient air of Delhi. *Atmos Environ* 2005; **39**: 59–71.

12 Adgate JL, Goldstein BD, McKenzie LM. Potential public health hazards, exposures and health effects from unconventional natural gas development. *Environ Sci Technol* 2014; **48**: 8307–8320.

13 Pöschl U, Shiraiwa M. Multiphase chemistry at the atmosphere-biosphere interface influencing climate and public health in the anthropocene. *Chem Rev* 2015; **115**: 4440–4475.

14 Dhada I, Sharma M, Nagar PK. Quantification and human health risk assessment of by-products of photo catalytic oxidation of ethylbenzene, xylene and toluene in indoor air of analytical laboratories. *J Hazard Mater* 2016; **316**: 1–10.

15 Haghighat F, Lee CS, Pant B, *et al.* Evaluation of various activated carbons for air cleaning – Towards design of immune and sustainable buildings. *Atmos Environ* 2008; **42**: 8176–8184.

16 Carter EM, Katz LE, Speitel Gerald E. J, *et al.* Gas-phase formaldehyde adsorption isotherm studies on activated carbon: correlations of adsorption capacity to surface functional group density. *Environ Sci Technol* 2011; **45**: 6498–6503.

17 Kołodziej A, Łojewska J. Optimization of structured catalyst carriers for VOC combustion. *Catal Today* 2005; **105**: 378–384.

18 Bo Z, Yang S, Kong J, *et al.* Solar-enhanced plasma-catalytic oxidation of toluene over a bifunctional graphene fin foam decorated with nanofin-like MnO_2. *ACS Catal* 2020; **10**: 4420–4432.

19 Feng X, Liu H, He C, *et al.* Synergistic effects and mechanism of a non-thermal plasma catalysis system in volatile organic compound removal: a review. *Catal Sci Technol* 2018; **8**: 936–954.

20 Zhan Y, Ji J, Huang H, *et al.* A facile VUV/H_2O system without auxiliary substances for efficient degradation of gaseous toluene. *Chem Eng J* 2018; **334**: 1422–1429.

21 Hoffmann MR, Martin ST, Choi W, *et al.* Environmental applications of semiconductor photocatalysis. *Chem Rev* 1995; **95**: 69–96.

22 Ilan YA, Czapski G, Meisel D. The one-electron transfer redox potentials of free radicals. I. The oxygen/superoxide system. *Biochim Biophys Acta* 1976; **430**: 209–224.

23 Frankcombe TJ, Smith SC. OH-initiated oxidation of toluene. 1. quantum chemistry investigation of the reaction path. *J Phys Chem A* 2007; **111**: 3686–3690.

24 Nosaka Y, Nosaka AY. Generation and detection of reactive oxygen species in photocatalysis. *Chem Rev* 2017; **117**: 11302–11336.

25 Weon S, Choi E, Kim H, *et al.* Active {001} facet exposed TiO_2 nanotubes photocatalyst filter for volatile organic compounds removal: from material development to commercial indoor air cleaner application. *Environ Sci Technol* 2018; **52**: 9330–9340.

26 Liang S, Shu Y, Li K, *et al.* Mechanistic insights into toluene degradation under VUV irradiation coupled with photocatalytic oxidation. *J Hazard Mater* 2020; **399**: 122967.

27 Zhang X, Wang L, Zhou X, *et al.* Investigation into the enhancement of property and the difference of mechanism on visible light degradation of gaseous toluene catalyzed by ZnAl layered double hydroxides before and after Au support. *ACS Sustain Chem Eng* 2018; **6**: 13395–13407.

28 Pei CC, Leung WWF. Photocatalytic oxidation of nitrogen monoxide and *o*-xylene by TiO_2/ZnO/Bi_2O_3 nanofibers: Optimization, kinetic modeling and mechanisms. *Appl Catal B-Environ* 2015; **174-175**: 515–525.

29 Hu Z, Yang C, Lv K, *et al.* Single atomic Au induced dramatic promotion of the photocatalytic activity of TiO_2 hollow microspheres. *Chem Commun* 2020; **56**: 1745–1748.

30 He F, Weon S, Jeon W, *et al.* Self-wetting triphase photocatalysis for effective and selective removal of hydrophilic volatile organic compounds in air. *Nat Commun* 2021; **12**: 6259.

31 Li J, Chen R, Cui W, *et al.* Synergistic photocatalytic decomposition of a volatile organic compound mixture: high efficiency, reaction mechanism, and long-term stability. *ACS Catal* 2020; **10**: 7230–7239.

32 Yang J, Wang X, Wang H, *et al.* $CsPbBr_3$ perovskite nanocrystal: A robust photocatalyst for realizing NO abatement. *ACS EST Eng* 2021; **1**: 1021–1027.

33 Schauer JJ, Fraser MP, Cass GR, *et al.* Source reconciliation of atmospheric gas-phase and particle-phase pollutants during a severe photochemical smog episode. *Environ Sci Technol* 2002; **36**: 3806–3814.

34 Elsayed N. Toxicity of nitrogen dioxide: an introduction. *Toxicology* 1994; **89**: 161–174.

35 Atkinson R. Atmospheric chemistry of VOCs and NO_x. *Atmos Environ* 2000; **34**: 2063–2101.

36 Nguyen VH, Nguyen BS, Huang CW, *et al.* Photocatalytic NO_x abatement: Recent advances and emerging trends in the development of photocatalysts. *J Clean Prod* 2020; **270**: 121912.

37 Granger P, Parvulescu VI. Catalytic NO_x abatement systems for mobile sources: from three-way to lean burn after-treatment technologies. *Chem Rev* 2011; **111**: 3155–3207.

38 Kim CH, Qi G, Dahlberg K, *et al.* Strontium-doped perovskites rival platinum catalysts for treating NO_x in simulated diesel exhaust. *Science* 2010; **327**: 1624–1627.

39 Hu P, Huang Z, Gu X, *et al.* Alkali-resistant mechanism of a hollandite DeNO_x catalyst. *Environ Sci Technol* 2015; **49**: 7042–7047.

40 Li K, Cui W, Li J, *et al.* Tuning the reaction pathway of photocatalytic NO oxidation process to control the secondary pollution on monodisperse Au nanoparticles@g-C_3N_4. *Chem Eng J* 2019; **378**: 122184.

41 Li J, Dong X, Sun Y, *et al.* Tailoring the rate-determining step in photocatalysis via localized excess electrons for efficient and safe air cleaning. *Appl Catal B-Environ* 2018; **239**: 187–195.

42 Dong X, Li J, Xing Q, *et al.* The activation of reactants and intermediates promotes the selective photocatalytic NO conversion on electron-localized Sr-intercalated g-C_3N_4. *Appl Catal B-Environ* 2018; **232**: 69–76.

43 Yang W, Ren Q, Zhong F, *et al.* Promotion mechanism of –OH group intercalation for NO_x purification on BiOI photocatalyst. *Nanoscale* 2021; **13**: 20601–20608.

44 Wang H, Li K, Li J, *et al.* Photochemical transformation pathways of nitrates from photocatalytic NO_x oxidation: implications for controlling secondary pollutants. *Environ Sci Technol Lett* 2021; **8**: 873–877.

45 Wang H, Sun Y, He W, *et al.* Visible light induced electron transfer from a semiconductor to an insulator enables efficient photocatalytic activity on insulator-based heterojunctions. *Nanoscale* 2018; **10**: 15513–15520.

46 Geng Q, Xie H, Cui W, *et al.* Optimizing the electronic structure of BiOBr nanosheets via combined Ba doping and oxygen vacancies for promoted photocatalysis. *J Phys Chem C* 2021; **125**: 8597–8605.

47 Geng Q, Xie H, He Y, *et al.* Atomic interfacial structure and charge transfer mechanism on *in-situ* formed BiOI/$Bi_2O_2SO_4$ p-n heterojunctions with highly promoted photocatalysis. *Appl Catal B-Environ* 2021; **297**: 120492.

48 Huo WC, Dong X, Li JY, *et al.* Synthesis of Bi_2WO_6 with gradient oxygen vacancies for highly photocatalytic NO oxidation and mechanism study. *Chem Eng J* 2019; **361**: 129–138.

49 Lei B, Cui W, Sheng J, *et al.* Synergistic effects of crystal structure and oxygen vacancy on Bi_2O_3 polymorphs: intermediates activation, photocatalytic reaction efficiency, and conversion pathway. *Sci Bull* 2020; **65**: 467–476.

50 Chen P, Dong F, Ran M, *et al.* Synergistic photo-thermal catalytic NO purification of MnO/g-C_3N_4: Enhanced performance and reaction mechanism. *Chin J Catal* 2018; **39**: 619–629.

51 Li J, Ran M, Chen P, *et al.* Controlling the secondary pollutant on B-doped g-C_3N_4 during photocatalytic NO removal: a combined DRIFTS and DFT investigation. *Catal Sci Technol* 2019; **9**: 4531–4537.

52 Ran M, Li J, Cui W, *et al.* Efficient and stable photocatalytic NO removal on C self-doped g-C_3N_4 : electronic structure and reaction mechanism. *Catal Sci Technol* 2018; **8**: 3387–3394.

53 Shang H, Li M, Li H, *et al.* Oxygen vacancies promoted the selective photocatalytic removal of NO with blue TiO_2 via simultaneous molecular oxygen activation and photogenerated hole annihilation. *Environ Sci Technol* 2019; **53**: 6444–6453.

54 Duan Y, Luo J, Zhou S, *et al.* TiO_2-supported Ag nanoclusters with enhanced visible light activity for the photocatalytic removal of NO. *Appl Catal B-Environ* 2018; **234**: 206–212.

55 Cui W, Yang W, Chen P, *et al.* Earth-abundant $CaCO_3$ -based photocatalyst for enhanced ROS production, toxic by-product suppression, and efficient no removal. *Energy Environ Mater* 2021; https://doi/org/10.1002/eem2.12214.

56 Wang H, Cui W, Dong X, *et al.* Interfacial activation of reactants and intermediates on $CaSO_4$ insulator-based heterostructure for efficient photocatalytic NO removal. *Chem Eng J* 2020; **390**: 124609.

57 Cui W, Chen L, Li J, *et al.* Ba-vacancy induces semiconductor-like photocatalysis on insulator $BaSO_4$. *Appl Catal B-Environ* 2019; **253**: 293–299.

58 Sun S, Ding J, Bao J, *et al.* Photocatalytic oxidation of gaseous formaldehyde on TiO_2: an *in situ* DRIFTS study. *Catal Lett* 2010; **137**: 239–246.

59 Zhu X, Jin C, Li XS, *et al.* Photocatalytic formaldehyde oxidation over plasmonic Au/TiO_2 under visible light: moisture indispensability and light enhancement. *ACS Catal* 2017; **7**: 6514–6524.

60 Li J, Cui W, Chen P, *et al.* Unraveling the mechanism of binary channel reactions in photocatalytic formaldehyde decomposition for promoted mineralization. *Appl Catal B-Environ* 2020; **260**: 118130.

61 Wang H, Dong X, Tang R, *et al.* Selective breakage of C-H bonds in the key oxidation intermediates of gaseous formaldehyde on self-doped $CaSn(OH)_6$ cubes for safe and efficient photocatalysis. *Appl Catal B-Environ* 2020; **277**: 119214.

62 He Y, Li J, Sheng J, *et al.* Crystal-structure dependent reaction pathways in photocatalytic formaldehyde mineralization on $BiPO_4$. *J Hazard Mater* 2021; **420**: 126633.

63 Huang Q, Hu Y, Pei Y, *et al. In situ* synthesis of TiO_2@NH_2-MIL-125 composites for use in combined adsorption and photocatalytic degradation of formaldehyde. *Appl Catal B-Environ* 2019; **259**: 118106.

64 Hu C, Tsai WF, Wei WH, *et al.* Hydroxylation and sodium intercalation on g-C_3N_4 for photocatalytic removal of gaseous formaldehyde. *Carbon* 2021; **175**: 467–477.

65 Zhu M, Muhammad Y, Hu P, *et al.* Enhanced interfacial contact of dopamine bridged melamine-graphene/TiO_2 nanocapsules for efficient photocatalytic degradation of gaseous formaldehyde. *Appl Catal B-Environ* 2018; **232**: 182–193.

66 Ran M, Cui W, Li K, *et al.* Light-induced dynamic stability of oxygen vacancies in $BiSbO_4$ for efficient photocatalytic formaldehyde degradation. *Energy Environ Mater* 2022; **5**: 305–312.

67 Chen Z, Peng Y, Chen J, *et al.* Performance and mechanism of photocatalytic toluene degradation and catalyst regeneration by thermal/UV treatment. *Environ Sci Technol* 2020; **54**: 14465–14473.

68 Li J, Dong X, Zhang G, *et al.* Probing ring-opening pathways for efficient photocatalytic toluene decomposition. *J Mater Chem A* 2019; **7**: 3366–3374.

69 Yang W, Cui W, Yang L, *et al.* The structural differences of perovskite $ATiO_3$ (A=Ca, Sr) dictate the photocatalytic VOCs mineralization efficiency. *Chem Eng J* 2021; **425**: 130613.

70 Wang J, Li J, Yang W, *et al.* Promote reactants activation and key intermediates formation for facilitated toluene photodecomposition via Ba active sites construction. *Appl Catal B-Environ* 2021; **297**: 120489.

71 Chen L, Chen P, Wang H, *et al.* Surface Lattice Oxygen Activation on $Sr_2Sb_2O_7$ Enhances the Photocatalytic Mineralization of Toluene: from Reactant Activation, Intermediate Conversion to Product Desorption. *ACS Appl Mater Interfaces* 2021; **13**: 5153–5164.

72 Liu Y, Chen S, Li K, *et al.* Promote the activation and ring opening of intermediates for stable photocatalytic toluene degradation over Zn-Ti-LDH. *J Colloid Interface Sci* 2022; **606**: 1435–1444.

73 Chen P, Cui W, Wang H, *et al.* The importance of intermediates ring-opening in preventing photocatalyst deactivation during toluene decomposition. *Appl Catal B-Environ* 2020; **272**: 118977.

74 Li K, He Y, Li J, *et al.* Identification of deactivation-resistant origin of $In(OH)_3$ for efficient and durable photodegradation of benzene, toluene and their mixtures. *J Hazard Mater* 2021; **416**: 126208.

75 Qu W, Wang P, Gao M, *et al.* Delocalization effect promoted the indoor air purification via directly unlocking the ring-opening pathway of toluene. *Environ Sci Technol* 2020; **54**: 9693–9701.

76 Chen R, Li J, Sheng J, *et al.* Unveiling the unconventional roles of methyl number on the ring-opening barrier in photocatalytic decomposition of benzene, toluene and *o*-xylene. *Appl Catal B-Environ* 2020; **278**: 119318.

77 Yang L, Guo J, Yang T, *et al.* Self-assembly Cu_2O nanowire arrays on Cu mesh: a solid-state, highly-efficient, and stable photocatalyst for toluene degradation under sunlight. *J Hazard Mater* 2021; **402**: 123741.

78 Lei B, Cui W, Chen P, *et al.* Rational design of LDH/Zn_2 SnO_4 heterostructures for efficient mineralization of toluene through boosted interfacial charge separation. *Energy Environ Mater* 2022; https://doi/org/10.1002/eem2.12291.

79 Paz Y. Application of TiO_2 photocatalysis for air treatment: Patents' overview. *Appl Catal B-Environ* 2010; **99**: 448–460.

80 Gandolfo A, Bartolomei V, Gomez Alvarez E, *et al.* The effectiveness of indoor photocatalytic paints on NO_x and HONO levels. *Appl Catal B-Environ* 2015; **166-167**: 84–90.

81 Jiang Q, Qi T, Yang T, *et al.* Ceramic tiles for photocatalytic removal of NO in indoor and outdoor air under visible light. *Building Environ* 2019; **158**: 94–103.

82 Yu B, Hou J, He W, *et al.* Study on a high-performance photocatalytic-Trombe wall system for space heating and air purification. *Appl Energy* 2018; **226**: 365–380.

83 Xu T, Zheng H, Zhang P. Performance of an innovative VUV-PCO purifier with nanoporous TiO_2 film for simultaneous elimination of VOCs and by-product ozone in indoor air. *Building Environ* 2018; **142**: 379–387.

84 Sánchez B, Sánchez-Muñoz M, Muñoz-Vicente M, *et al.* Photocatalytic elimination of indoor air biological and chemical pollution in realistic conditions. *Chemosphere* 2012; **87**: 625–630.

85 Kim S, Kim S, Park HJ, *et al.* Practical scale evaluation of a photocatalytic air purifier equipped with a Titania-zeolite

composite bead filter for VOC removal and viral inactivation. *Environ Res* 2022; **204**: 112036.

86 Martínez-Montelongo JH, Medina-Ramírez IE, Romo-Lozano Y, *et al.* Development of a sustainable photocatalytic process for air purification. *Chemosphere* 2020; **257**: 127236.

87 Zhong L, Haghighat F. Photocatalytic air cleaners and materials technologies—Abilities and limitations. *Building Environ* 2015; **91**: 191–203.

88 Hanus MJ, Harris AT. Nanotechnology innovations for the construction industry. *Prog Mater Sci* 2013; **58**: 1056–1102.

89 Gopalan AI, Lee JC, Saianand G, *et al.* Recent progress in the abatement of hazardous pollutants using photocatalytic TiO_2-based building materials. *Nanomaterials* 2020; **10**: 1854.

90 Chen M, Liu Y. NO_x removal from vehicle emissions by functionality surface of asphalt road. *J Hazard Mater* 2010; **174**: 375–379.

91 Chen M, Chu JW. NO_x photocatalytic degradation on active concrete road surface—from experiment to real-scale application. *J Clean Prod* 2011; **19**: 1266–1272.

92 Guerrini GL. Photocatalytic performances in a city tunnel in Rome: NO_x monitoring results. *Constr Build Mater* 2012; **27**: 165–175.

93 Costa A, Chiarello GL, Selli E, *et al.* Effects of TiO_2 based photocatalytic paint on concentrations and emissions of pollutants and on animal performance in a swine weaning unit. *J Environ Manage* 2012; **96**: 86–90.

94 Lettieri M, Colangiuli D, Masieri M, *et al.* Field performances of nanosized TiO_2 coated limestone for a self-cleaning building surface in an urban environment. *Building Environ* 2019; **147**: 506–516.

95 Le Pivert M, Kerivel O, Zerelli B, *et al.* ZnO nanostructures based innovative photocatalytic road for air purification. *J Clean Prod* 2021; **318**: 128447.

96 Fu Q, Liu Y, Mo J, *et al.* Improved capture and removal efficiency of gaseous acetaldehyde by a self-powered photocatalytic system with an external electric field. *ACS Nano* 2021; **15**: 10577–10586.